Biochimica et Biophysica Acta 1808 (2011) 792–801

Contents lists available at ScienceDirect

Biochimica et Biophysica Acta

journal homepage: www.elsevier.com/locate/bbamem

Manipulation of cell volume and membrane pore comparison following single cell permeabilization with 60- and 600-ns electric pulses

Olena M. Nesin [a], Olga N. Pakhomova [a], Shu Xiao [a,b], Andrei G. Pakhomov [a,*]

[a] Frank Reidy Research Center for Bioelectrics, Old Dominion University, Norfolk, VA, USA
[b] Department of Electrical and Computer Engineering, Old Dominion University, Norfolk, VA, USA

ARTICLE INFO

Article history:
Received 8 November 2010
Received in revised form 11 December 2010
Accepted 14 December 2010
Available online 20 December 2010

Keywords:
Membrane permeability
Colloid osmotic effect
Pore size
Nanopores
Nanosecond pulses
Electroporation

ABSTRACT

Intense nanosecond-duration electric pulses (nsEP) open stable nanopores in the cell membrane, followed by cell volume changes due to water uptake or expulsion, as regulated by the osmolality balance of pore-impermeable solutes inside and outside the cell. The size of pores opened by either fifty 60-ns EP (~13 kV/cm) or five, 600-ns EP (~6 kV/cm) in GH3 cells was estimated by isoosmotic replacement of bath NaCl with polyethylene glycols and sugars. Such replacement reduced cell swelling or resulted in transient or sustained cell shrinking in response to EP. depending on the availability of pores permeable to the test solute. Unexpectedly, solute substitutions showed that for the same integral area of pores opened by 60- and 600-ns treatments (as estimated by cell volume changes), the pore sizes were similar. However, the 600-ns exposure triggered significantly higher cell uptake of propidium. We concluded that 600-ns EP opened a greater number of larger (propidium-permeable pores), but the fraction of the larger pores in the entire pore population was insufficient to contribute to cell volume changes. For both the 60- and 600-ns exposures, cell volume changes were determined by pores smaller than 0.9 nm in diameter; however, the diameter increased with increasing the nsEP intensity.

1. Introduction

The phenomenon of cell membrane permeabilization by intense electric pulses, or electroporation, has been extensively studied during recent decades [1–7]. Although most studies concur that electropermeabilization results from formation of long-lived hydrophilic pores in the lipid bilayer, the exact nature of such pores, their structure and mechanisms that control pore size and resealing remain poorly understood. Nonetheless, electropermeabilization is used widely for intracellular delivery of substances and genes, as well as for tissue and tumor destruction [8–12].

Membrane permeabilization can be conveniently visualized by uptake of fluorescent dyes that do not pass through the intact membrane, with propidium (Pr) iodide being by far the most popular [13–16]. Pr uptake assay is simple, reliable, and exerts high sensitivity due to profound enhancement of fluorescence upon Pr binding to nucleic acids. In multiple electroporation studies, Pr uptake was employed as a sole and self-sufficient criterion of pore formation and/or of cell death. (Notably, propidium iodide (PI) dissociates in water, and cell staining is determined by the passage of Pr^{2+} (not of the entire PI molecule) through membrane pores. The traditional terminology (e.g., "PI uptake" and "PI fluorescence") becomes misleading when talking about the size of the pores [17,18], so we use the abbreviation "Pr" instead.)

Pore size and number are perhaps two major endpoints that determine permeabilization efficiency, physiological effects, and eventual cell survival after the treatment. In early studies, the pore size estimates fell in a rather wide range, roughly from 1 to 100 nm [19–21]. Despite such variability, it has been generally recognized that longer and more intense pulses open larger pores. Specifically, the shortest pulses tested at that time (0.5 μs) opened the smallest pores permeable to Rb^+, but not to any larger solutes [22].

It was not until mid-90s when ultra-short pulse exposure technologies became available, and bioeffects of nanosecond electric pulses (nsEP) received much attention. Equivalent circuit modeling suggested that nsEP could potentially bypass the plasma membrane and reach cell interior, thereby targeting organelles and porating internal membranes [23,24]. This idea was corroborated by multiple reports of nsEP bioeffects which were not accompanied by Pr entry [15,25,26]; however, these studies overlooked the possibility that nsEP-opened plasma membrane pores could be smaller than needed for Pr cation passage (about 1.5 nm [17,18]).

Indeed, opening of small plasma membrane pores in nsEP-treated cells has later been revealed by patch clamp [27–30] and by fluorescent detection of Tl^+ uptake and Yo-PRO-1 dye uptake

Abbreviations: EP, electric pulses; nsEP, nanosecond-duration electric pulses; PEGs, polyethylene glycols; Pr, propidium

* Corresponding author. Frank Reidy Research Center for Bioelectrics, Old Dominion University, 4211 Monarch Way, Suite 300, Norfolk, VA 23508, USA. Tel.: +1 757 683 8003; fax: +1 757 314 2397.
E-mail address: andrei@pakhomov.net (A.G. Pakhomov).

0005-2736/$ – see front matter © 2010 Elsevier B.V. All rights reserved.
doi:10.1016/j.bbamem.2010.12.012

[17,18,27,31]. Since both Yo-PRO-1 and Tl^+ are smaller than Pr, the exclusion of the latter by nsEP-treated cells has set an estimate of the upper limit of pore size at 1–1.5 nm. These experimental data were consistent with more advanced theoretical models that predicted large quantities of small pores both in the plasma membrane and in the internal membranes [32]. The term "nanopores" was introduced to distinguish the smallest population of electropores from larger pores that are produced by conventional electroporation with longer pulses [17,18,27,31,33].

In actuality, nanopore size estimates based on differential uptake of fluorescent dyes are limited by dye selections and confounded by differences in the emission efficiency and detector sensitivity. Increasing nsEP intensity (either E-field or pulse number) and boosting fluorescence detector sensitivity far above the values needed for routine live/dead cell distinction can reliably reveal nsEP-triggered Pr uptake, albeit usually weak [17,18,27]. Although electropores are not rigid structures and are likely to experience thermal and stochastic size fluctuations, the observations of Pr uptake have somewhat blurred the alleged difference between the nano- and conventional pore categories. At present, no experimental data are available to prove that reduction of pulse duration from hundreds to tens of nanoseconds and even less would produce still smaller pores. Alternatively, one can expect that there is a certain minimum size limit required for stable nanopore formation (at room temperature, the lifetime of nanopores is on the order of minutes [1,17,18,27,29,33]).

The goal of the present study was to compare nanopore populations created by 60- and 600-ns pulses. Instead of relying solely on the fluorescent dye uptake, we employed a potentially more accurate pore size estimation method based on cell volume manipulation following plasma membrane permeabilization [17,19–21,34–36].

The basis for this method is a well-documented phenomenon of cell volume change (typically, cell swelling) following nsEP exposure [17,28]. Presumably the principal driving force for nsEP-initiated water uptake is a so-called colloid osmotic mechanism [17,21,37]. In brief, small intra- and extracellular solutes will travel freely across the plasma membrane of a porated cell, to approach the concentration, electrochemical, and osmotic equilibrium. At the same time, larger intracellular solutes (unable to pass through membrane pores) will be trapped inside, creating additional osmotic pressure and attracting water to cause cell swelling. However, swelling will be suppressed or replaced by shrinking if the bath buffer contains a sufficient amount of large (i.e., pore-impermeable) solutes to counterbalance the osmotic pressure of large solutes inside the cell.

Hence, the pore size can be estimated by isoosmotic replacement of small solutes in the bath (typically, Na^+ and Cl^-) with various larger solutes, like polyethylene glycols (PEGs) or neutral sugars. Once the size of the test solute prohibits it from going through pores, nsEP-induced cell swelling will be replaced with shrinking, so the pore size can be estimated from the solute's molecular dimensions. PEGs have been particularly popular as a test solute, as they form in water a random-shaped coil with the radius proportional to their molecular weight [34,35,38].

Notably, intermediate-sized solutes might be able to enter the cell through pores, but this process takes significant time. As a result, such solutes may cause transient cell shrinking, which eventually stops and is followed by swelling when the test solute accumulates in the cell. Such biphasic effects will be illustrated and discussed below in this paper.

Earlier studies that utilized the colloid osmotic mechanism for pore size estimation relied on "bulk" measurements of cell volume, e.g., on light scattering by a cell suspension or on eventual lysis of permeabilized cells [19–22,36]. While these studies produced important estimations of the electropores size and lifetime, the findings were somewhat ambiguous. Light scattering could be profoundly affected by blebbing and cytoplasm granulation [17,28], which would interfere with volume estimates. Eventual lysis of electroporated cells could be conveniently measured in erythrocytes, but not in most other cell lines that lack a colored pigment; this method also assumes the lack of pore size changes or resealing during the observation period of 10–20 h, and bears no information on the time dynamics of volume changes. As a more rigorous alternative to the "bulk" methods, in this study we measured cell volume in individually electroporated cells using a multiple-plane, time-lapse confocal imaging and subsequent 3D cell reconstruction. In addition, we performed experiments both with different PEGs and different sugars, in order to verify that their effects are related to the ability to pass through the pores, rather than to specific chemical properties.

2. Materials and methods

2.1. Cell line and propagation

We used GH3 cells (rat pituitary) obtained from ATCC (Manassas, VA). This cell line has been extensively used in nsEP studies [17,27,29,30]; it has small size and nearly round shape which facilitate the 3D volume reconstruction. Cells were propagated at 37°C with 5% CO_2 in air in Ham's F12K medium supplemented with 2.5% fetal bovine serum, 15% horse serum, and 1% penicillin/streptomycin. The cell culture components were obtained from Atlanta Biologicals (Norcross, GA) or Mediatech Cellgro (Herndon, VA.) For the passage immediately preceding the experiments, cells were transferred onto glass coverslips pre-treated with poly-L-lysine (Sigma-Aldrich, St. Louis, MO) to improve cell adhesion.

2.2. Cell imaging and volume measurements

To mark the cell volume for confocal imaging, cells were loaded with a fluorescent indicator Cell Tracker™ Green CMFDA (5-chloromethylfluorescein dictate, Invitrogen, Eugene, OR). Cell loading and handling protocols were modified from [39]. A 10-mM DMSO stock of Green CMFDA ester was diluted to 4.5 μM in the loading buffer composed of (in mM): 130 NaCl, 5 KCl, 2 $MgCl_2$, 2 $CaCl_2$, 10 HEPES, and 10 glucose (pH 7.4). Cells were loaded with the dye by incubation in this buffer for 20–25 min at room temperature. After loading, cells were returned into the growth medium and allowed to recover in the incubator for 30–60 min prior to being used in experiments. The loading buffer (without the dye) was also used to rinse the coverslip between any changes of the media.

A coverslip with dye-loaded cells was placed into a glass-bottomed chamber (Warner Instruments, Hamden, CT) mounted on an Olympus IX71 inverted microscope equipped with an FV 300 confocal laser scanning system (Olympus America, Center Valley, PA).

The dye was excited at 488 nm and its emission was detected in the band from 510 to 530 nm. Stacks of XY scans through the entire depth of the cell (typically, 12–15 Z-sections at 1.4-μm steps, starting from within the coverslip and going upward) were obtained repeatedly with 30-s intervals; three stacks were recorded prior to nsEP exposure (baseline), followed by 15–20 identical stacks after nsEP exposure or a sham exposure. To minimize distortion due to fluorescence "bleeding" into Z-planes above and below the confocal plane, we used a 60×, 1.42 NA oil objective and the smallest confocal aperture.

The time-lapse image acquisition and Z-direction stepping of the objective were programmed in FluoView V. 5.0 software (Olympus). 3D reconstruction of Z-stacks and volume measurements were accomplished with a SlideBook 5.0 (Olympus). The cells chosen for experiments were round-shaped, free of visible defects, and had a cell volume of 1916 +/- 62 μm^3 (mean +/- S.E., based on $n = 50$) Quantitative data were corrected for dye bleaching and expressed as a change (%) from the initial (pre-exposure) cell volume. Due to multiple statistical comparisons made (exposures versus controls; 60-ns versus 600-ns treatments; pre-exposure versus post-exposure

time points; different bath buffers to each other; etc.), we chose to let the error bars in graphs speak for the statistical difference without using asterisks or other special symbols. However, when it was critical for data interpretation, we emphasized the significant differences (or lack thereof) in the body text and figure captions.

2.3. Propidium uptake

Cell handling procedures were the same as described above, except for the omission of the CellTracker dye loading. Propidium iodide (Sigma-Aldrich) at 30 μg/ml was added to the reference buffer (see below). Florescent images from a single Z-plane, presumably half-way through the cell, were collected every 10 s using a large confocal aperture (excitation: 488 nm; emission 605 nm). Photomultiplier tube settings were biased towards high sensitivity and detection of even minimal Pr uptake. Images were quantified with MetaMorph v. 7.5 (MDS, Foster City, CA).

2.4. Chemicals and buffers

A reference buffer for measuring nsEP effect on cell volume contained (in mM): 135 NaCl, 5 KCl, 4 $MgCl_2$, 3 HEPES, 10 glucose, and 2 Na-EGTA (pH 7.4). External Ca^{2+} was omitted in order to minimize multiple physiological effects that could be triggered by Ca^{2+} entry through electropores, including pore repair by endo- and exocytosis [40,41] and active volume regulation [37]. Since the overall concentration of bivalent cations is important for membrane stability [42], Mg^{2+} concentration was raised to 4 mM to compensate for the lack of Ca^{2+}.

In experiments with different sugars, 100 mM of NaCl in the reference buffer was isoosmotically replaced with a sugar (180 mM of adonitol, methyl-α-D-glucoside, D-mannitol, or sucrose).

Buffers containing PEGs were formulated similarly; however, isoosmotic PEGs' concentrations had to be found by trial and error. PEGs exhibit a peculiar dependence of their osmolality upon both their molecular size and concentration [35,43]. When NaCl concentration in the reference buffer was dropped to 35 mM, the overall osmolality was brought back to ~300 mOsm/kg by the addition of PEG 200 at 162 mM, PEG 300 at 152 mM, PEG 400 at 134 mM, PEG 600 at 105 mM, PEG 1000 at 83 mM, or PEG 4000 at 26 mM. Isolated experiments that used PEGs at different concentrations and osmolalities are identified as such below.

The osmolality of all solutions was between 290 and 310 mOsm, as measured with a freezing point microosmometer (Advanced Instruments, Inc., Norwood, MA). Out of this number, about 190 mOsm/kg was contributed by PEGs or sugars. This value was intended to markedly exceed the osmolality of pore-impermeable intracellular solutes, thereby resulting in cell shrinking if a particular PEG or sugar was too large to enter the cell through electropores. In control experiments without nsEP stimulation, none of the tested buffers had a significant effect on the cell volume.

Chemicals were purchased from Sigma-Aldrich or Qiagen (Valencia, CA). All buffers were used at a room temperature of 22–24 °C.

2.5. Nanosecond pulse stimulation and local electric field modeling

The method of nsEP exposure of individual cells on a coverslip was the same as described recently [27,30]. Nearly rectangular 60- or 600-ns pulses were generated in a transmission line-type circuit, by closing a MOSFET switch upon a timed delivery of a TTL trigger pulse from pClamp software via a Digidata 1322A output (MDS). The same devices were employed to synchronize the acquisition of cell images with nsEP exposure and buffer exchanges (when necessary).

NsEP were delivered to a selected cell with a pair of tungsten rod electrodes (0.08-mm diameter, 0.15–0.23 mm gap). With a help of a robotic manipulator (MP-225, Sutter, Novato, CA), these electrodes were positioned precisely at 50 μm above the coverslip surface so that the selected cell was in the middle of the gap between their tips. The E-field at the cell location was determined by 3D simulations with a finite element Maxwell equations solver Amaze 3D (Field Precision, Albuquerque, NM). The exact nsEP shapes and amplitudes were captured and measured with a 5-GHz TDS 3052 oscilloscope (Tektronix, Beaverton, OR). In most experiments, we exposed cells either to a 1-Hz train of five 600-ns pulses, or to a 10-Hz train of fifty 60-ns pulses; therefore, the train durations were the same, whereas the pulse amplitudes were adjusted to produce equal effects (see below).

2.6. Experiment strategy and protocols

The 60- and 600-ns treatment protocols were empirically established in preliminary experiments. The goal was to make the treatment intense enough to cause well-measurable cell swelling (in the reference buffer), but not too severe to destroy the cells within a 10-min observation period. The treatments were made similar in the overall duration and the cumulative duration when the E-field was on (five 600-ns pulses at 1 Hz and fifty 60-ns pulses at 10 Hz). The E-field amplitude was fine tuned, by trial and error, so that cells exposed to either 600- or 60-ns trains exhibited a similar degree of swelling in the reference buffer. Since this buffer contained mostly small (presumably pore-permeable) solutes, the similarity of swelling indicated that the integral area of all pores opened by 60- and 600-ns treatments was also the same. However, the same integral area could result from opening of either the same number of similarly sized pores, or of a larger number of smaller pores. In case of the same number of similarly sized pores, PEGs and sugars would inhibit cell swelling to the same extent after 600- and 60-ns pulses. However, in case of a pore size difference, e.g., in case of smaller pores opening by 60-ns pulses, smaller PEGs and sugars will be more efficient in blocking cell swelling caused by 60-ns pulses.

Within each series of experiments, different exposures were randomized and accompanied by "sham" exposures (same procedures, but excluding nsEP delivery). As a rule, each treatment was independently tested in 4–10 individual cells from different batches.

2.7. Molecular dimensions

The radius of a PEG random coil is related to its molecular weight through the so-called Kuga relation [38]. In this study, we used PEG hydrodynamic diameter values as estimated by viscosity measurements for buffer conditions similar to ours [34]: PEG 200, 0.91 nm; PEG 400, 1.24 nm; PEG 600, 1.5 nm; PEG 1000, 1.9 nm. Although different size PEGs have been often employed for pore sizing both in artificial lipid bilayers and in living cells [34,35,44,45], one should note that the hydrodynamic diameter is not necessarily an accurate metric that defines their ability to pass through a pore.

For tested sugars, 3D atomic coordinates were calculated using CORINA program [46] and linear codes in a SMILES format extracted from PubChem database (http://pubchem.ncbi.nlm.nih.gov/search). Molecular dimensions were calculated with MOLEMAN2 software [47], http://xray.bmc.uu.se/usf/, and Van der Waals radii of singly bonded hydrogens (1.17 A) were added at each end to determine the impenetrable molecular volume [48]. Molecular views of the sugars (Fig. 1) were obtained using Jmol open-source Java viewer for chemical structures in 3D, http://www.jmol.org/.

The diameter of unhydrated molecules is often expressed as the geometric mean of the three orthogonal dimensions [21,49,50]; these numbers are provided in Fig. 1. However, for a molecule with substantially different dimensions in different planes, the ability to pass through a pore will likely be determined by the minimum molecular cross-section, rather than by the largest dimension of that molecule. Assuming round shape of an electropore, its diameter should be large enough to accommodate the two smaller dimensions of any (unhydrated) permeant molecule (see [49] for more discussion). To find

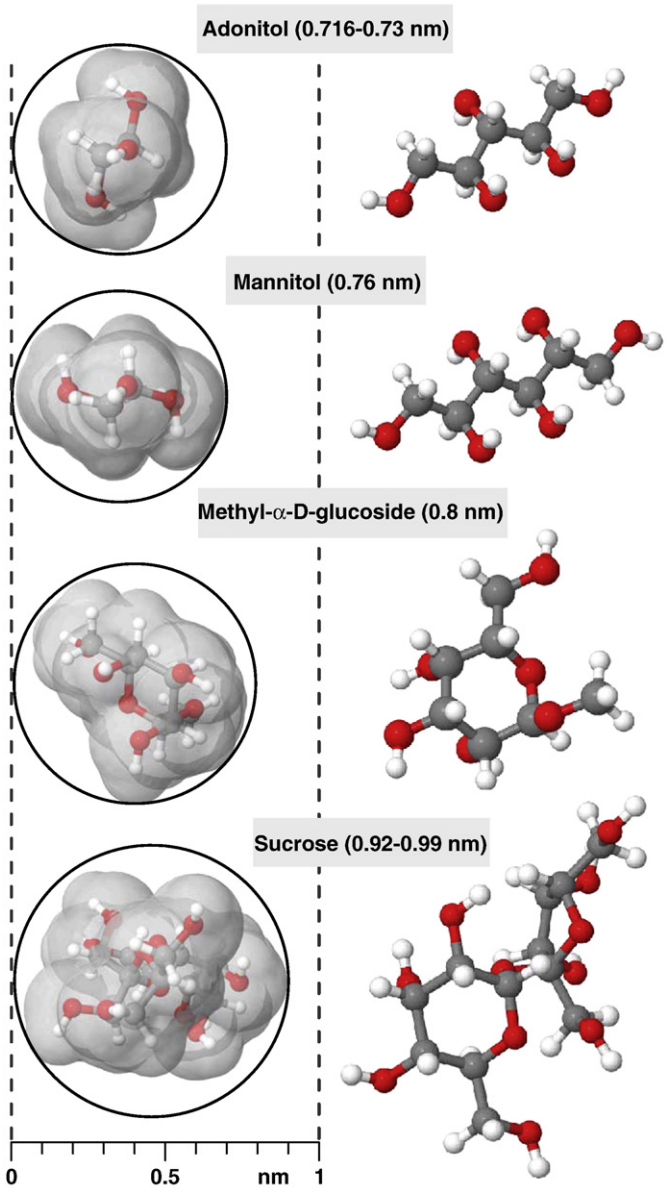

Fig. 1. Minimum molecular cross-sections of tested sugars and their molecular structures. Gray areas in the cross-section views (left column) limit the impenetrable molecular volume. The numbers following the names of the sugars correspond to the geometric mean of the three orthogonal molecular dimensions; two values are given in case of differently sized isomers. See text for more detail.

this diameter, the molecular shapes of the tested sugars were rotated in the Jmol viewer until finding the molecular projection corresponding to the minimum cross-section of the molecule (Fig. 1, left column); gray areas show van der Waals surface of the impenetrable molecular volume [48]. When a tested sugar might be present in the buffer in different isomeric forms, the smaller isomer was used for graphing. In actuality, the effective size of sugar molecules could be somewhat increased by hydration; however, the potential impact of hydration is difficult to estimate [42] and was beyond the scope of this paper.

3. Results

3.1. Measurements of nsEP-induced cell volume change and the effect of pore-impermeable solutes

As a first step, we selected nsEP parameters to cause well-measurable cell swelling in the reference buffer. We also verified that an isoosmotic replacement of the bath NaCl with a larger solute reverts swelling into shrinking, consistently with what was expected from the colloid osmotic mechanism.

Fig. 2A shows selected confocal fluorescent images of a cell before nsEP exposure and at different time intervals after it. The cell was kept in the reference buffer, and nsEP-induced swelling is seen as a gradual enlargement of the fluorescence area in all Z-slices. Fig. 2B shows another cell that developed a large bleb following nsEP exposure. Blebbing would have unpredictable results on cell volume measurements by indirect methods such as light scattering, but posed no problem for 3D volume reconstruction. Finally, Fig. 2C illustrates that the same nsEP exposure as in (A) caused shrinking instead of swelling when a portion of NaCl in the bath buffer was isoosmotically replaced with pore-impermeable PEG 4000.

Fig. 3 demonstrates that the inhibition of nsEP-induced cell swelling by PEG 4000 increased with increasing PEG concentration and osmolality. Cell swelling was unambiguously replaced with shrinking when PEG osmolality reached 190 mOsm/kg, which was therefore chosen for subsequent experiments.

3.2. Inhibition of cell swelling by PEGs of different molecular weight

Fig. 4 compares the effects of isoosmotic replacement of NaCl by different PEGs on cell volume changes triggered by 600- and 60-ns pulse exposures. Despite careful "tuning" of the pulse amplitude in preliminary experiments, swelling induced by 60-ns EP in the reference buffer happened to be slightly weaker than that of 600-ns EP; this inaccuracy was taken into account when interpreting the results.

As expected, swelling was gradually attenuated and replaced by shrinking as the molecular weight of PEG increased. For either 60- or 600-ns exposures, PEG 200 only reduced the rate of swelling, as compared with the reference NaCl buffer. With PEG 300, nsEP-induced swelling was replaced by a modest and transient shrinking, followed by cell volume increase at later time points. Same nsEP exposures in the presence of still larger PEGs caused lasting shrinking of exposed cells. The degree of shrinking was slightly higher after 600-ns exposures. This difference, however, can be adequately explained by the fact that the 60-ns exposure was slightly "weaker," i.e., it induced less volume change response in the reference buffer. Overall, the experiments with different PEGs produced no evidence that pores opened by 60-ns pulses are different from those opened by 600-ns pulses.

3.3. Inhibition of cell swelling by sugars

The experiment presented in Fig. 5 is similar to the one in Fig. 4, but different sugars were used instead of small PEGs. In additional experiments that preceded that main series and were not included in statistics, the amplitudes of 60- and 600-ns EP were further adjusted for better matching of their swelling effects in the reference buffer.

Smaller sugars (adonitol, mannitol, and methyl-α-D-glucoside) caused transient shrinking followed by swelling. Shrinking was more profound and transition to swelling occurred later when larger molecular weight sugars were used. This biphasic change of the cell volume can be readily explained by a slow (compared to Na^+ and Cl^-) but nonetheless significant entry of these sugars into electropermeabilized cells. At the early time points after nsEP, the osmotic pressure of sugars in the bath exceeded the osmotic pressure of pore-impermeable components inside the cell, thereby causing water loss and cell shrinking. With time, sugar molecules penetrated into the cell, gradually reducing their osmotic imbalance. Eventually, a point was reached when the osmotic pressure of pore-impermeable substances inside the cell became the driving force for water uptake and cell swelling. As one would expect, the transition from shrinking to swelling occurred later for larger sugar molecules that had lower

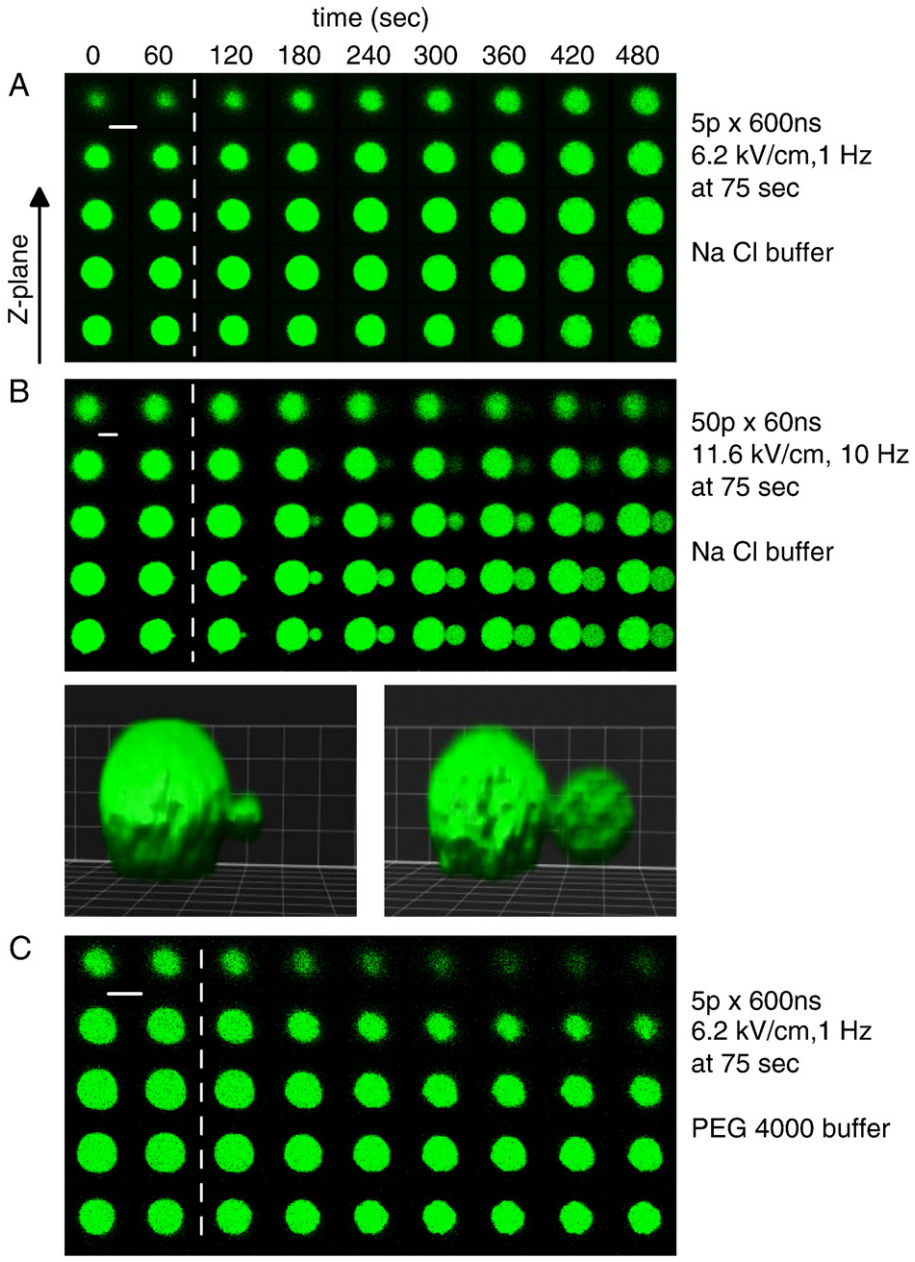

Fig. 2. Time-lapse confocal imaging of nsEP-treated cells. A–C: three representative experiments in individual GH3 cells. Columns correspond to different time points (60-s interval), and rows represent different Z-plane scans (2.8-μm distance). Scanning began from below the cell (within the coverslip) and continued upward until getting above the cell; for clarity, only several selected scans through the cell body are shown. Left two columns are the images taken prior to nsEP exposure (vertical dashed line). The exposure parameters and the pulsing buffer used are indicated next to the respective panels ("NaCl" is the reference buffer; "PEG 4000" is the same buffer with 100 mM of NaCl isoosmotically substituted for PEG 4000). Panel (B) also includes 3D reconstruction of the cell showing a growing bleb. Scale bars: 10 μm.

mobility and needed more time to enter the cell in appreciable amounts.

The largest sugar tested (sucrose) and PEG 1000 caused sustained cell shrinking that was not replaced by late swelling. This result suggests that both sucrose and PEG 1000 did not penetrate into the nsEP-exposed cells, or their uptake was too small for detection by the volume change-based method.

In either case, the effects of 60- and 600-ns pulse exposures were very similar. The magnitude and time dynamics of the cell volume change showed no statistically significant difference between two exposure conditions for any of the tested bath buffers. These data provided strong evidence that the size "profiles" of pore populations created by 60- and 600-ns pulses were essentially identical.

This unexpected finding was in contradiction both to the theoretical model predictions that shorter pulses should open smaller pores and to earlier observations using fluorescent dyes. Therefore, we decided to compare Pr uptake specifically for the exposure conditions that were used in cell volume change experiments.

3.4. Propidium uptake in nsEP-exposed cells

Pr uptake was quantified in GH3 cells exposed to 60- or 600-ns pulses in the reference buffer supplemented with 30 uM of propidium iodide (Fig. 6). Longer pulses induced significantly more Pr uptake; assuming that the total area of pores opened by 60- and 600-ns pulses was the same (see above), this finding indicates that the longer pulses produced greater number of pores of larger diameter. The rate of Pr uptake was the highest immediately after nsEP treatment and gradually slowed down.

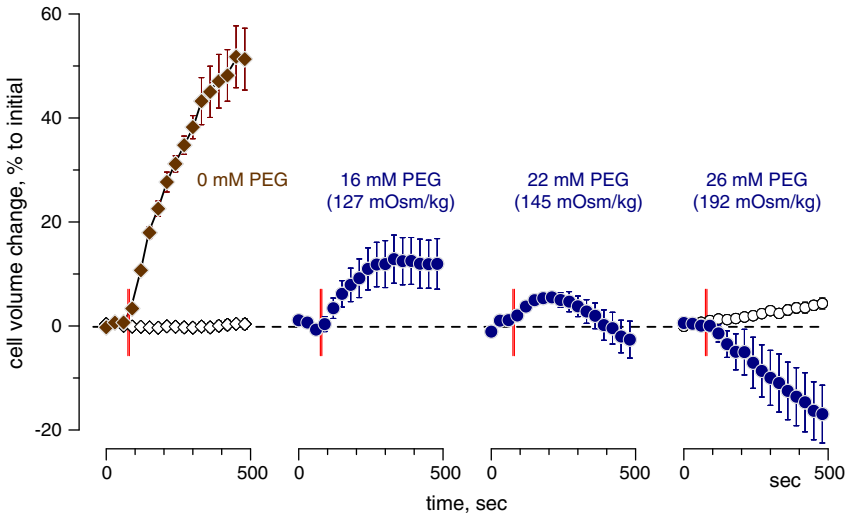

Fig. 3. Isoosmotic substitution of bath NaCl with PEG 4000 inhibits nsEP-induced cell swelling. Left panel: reference buffer (0 mM PEG); other panels: increasing fractions of PEG, as indicated above the graphs. Vertical lines denote nsEP exposure at 75 s into the experiments (5p × 600 ns, 1 Hz, 6.2 kV/cm; solid symbols) or sham exposures (open symbols). Mean ± SE, $n = 4–6$.

Thus, contrary to findings based on cell volume changes, Pr uptake suggested opening of larger pores when applying 600-ns pulses. Notably, Pr^{2+} is much larger than either sucrose or PEG 400, and the minimum cross-section of Pr-permeable pores was estimated at about 1.5 nm [17,18].

This apparent contradiction of the dye uptake data with the solute substitution experiments may imply (**a**) that larger, Pr-permeable pores shrink rapidly (within seconds), so the contribution of the pore size differences to cell volume changes is negligible, or (**b**) that the Pr-permeable pores represent just a small fraction of the total pore population opened by nsEP, so their impact on volume changes is insignificant. Continued increase of the Pr signal during minutes after exposure in Fig. 6 could be a sign of continued Pr uptake, but it could also be a result of continuing Pr binding to nucleic acids and resultant increase in its emission. Therefore the data presented in Fig. 6 provide no evidence to distinguish between the interpretations (**a**) and (**b**).

3.5. Effect of the E-field intensity on the pore size

Cell volume changes triggered by a 1-Hz train of five 600-ns pulses at 4, 6.2, or 12.4 kV/cm were measured in the reference buffer and in the same buffer containing 180 mM sucrose (NaCl was reduced to 35 mM to keep the overall osmolality unchanged). Sucrose was the smallest of the tested solutes that showed no signs of entry into cells under the exposure conditions employed above, and therefore was expected to be the most likely candidate to enter the pores in case of their enlargement by the higher E-field (Fig. 7).

Increasing of the E-field caused faster swelling in the reference buffer (NaCl) and faster shrinking in the sucrose buffer. The rate of early changes in the cell volume was quantified for the time interval from 90 to 120 s of the experiment (i.e., from 25 to 55 s from the start of exposure). In both buffers, the rate of the early changes increased proportionally to the E-field (Fig. 7B).

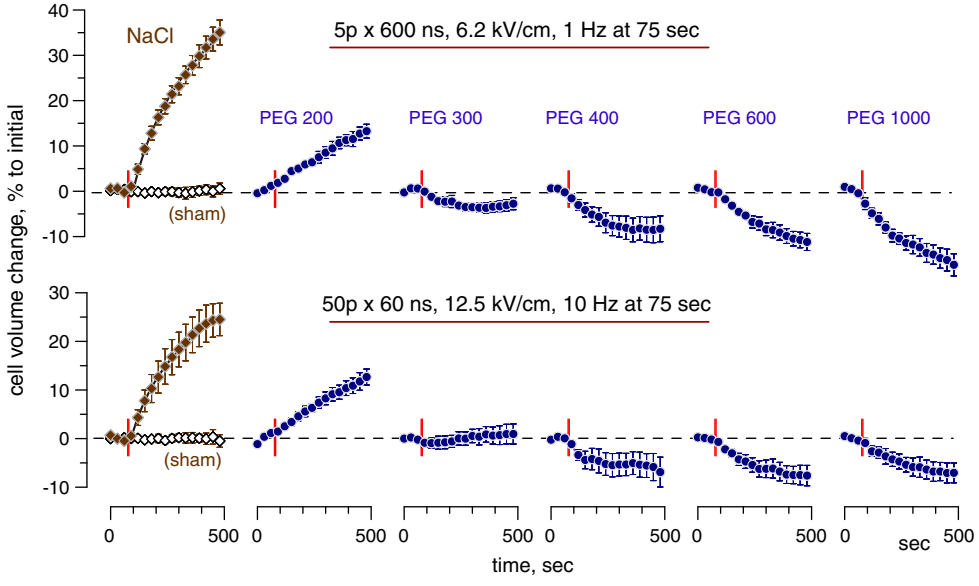

Fig. 4. Inhibition of nsEP-induced cell swelling by different PEGs is similar for 60- and 600-ns exposures. Molecular weights of tested PEGs and exposure parameters are shown above the graphs. "NaCl" denotes experiments in the reference buffer without PEG. The integral osmolality of all buffers is 290–300 mOsm/kg; out of this number, about 190 mOsm/kg is contributed by PEG (except "NaCl" group). Mean ± SE, $n = 4–7$. Cell volume fluctuations in sham-exposed cells in the PEG buffers were small (within -3% to 4% interval) and not statistically significant (data not shown for clarity). See Fig. 3 and text for more detail.

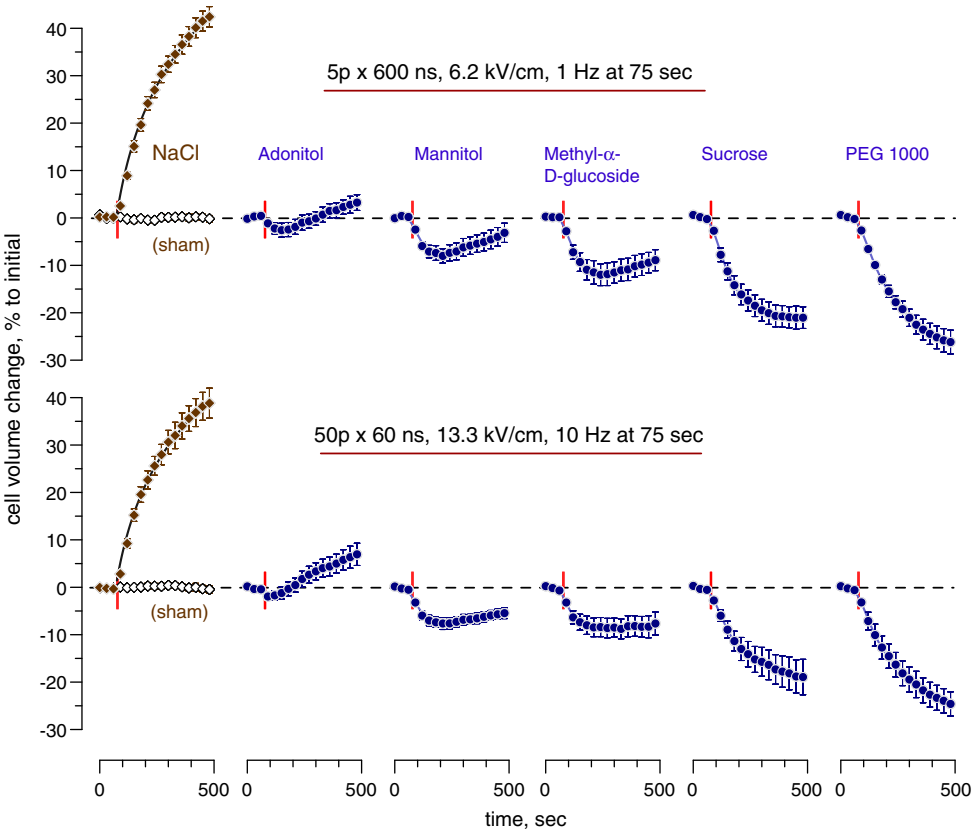

Fig. 5. The effect of sugars and PEG 1000 on the direction, amplitude, and time course of nsEP-induced cell volume changes depends on their molecular size, but is identical for 60- and 600-ns EP exposures. Mean ± SE, $n = 8–10$. Designations are the same as in Figs. 3 and 4. See text for more detail.

Cell volume kept changing at a gradually decreasing pace, with a notably different behavior of cells exposed in the sucrose buffer at the highest field intensity. In these cells, profound early shrinking has stopped soon, and later on was replaced by a modest, but statistically significant volume increase (Fig. 7C). Similarly to the data discussed above (Figs. 4 and 5), such biphasic response was caused by slow sucrose entry, thereby providing evidence for the formation of larger, sucrose-permeable pores at the highest tested field intensity.

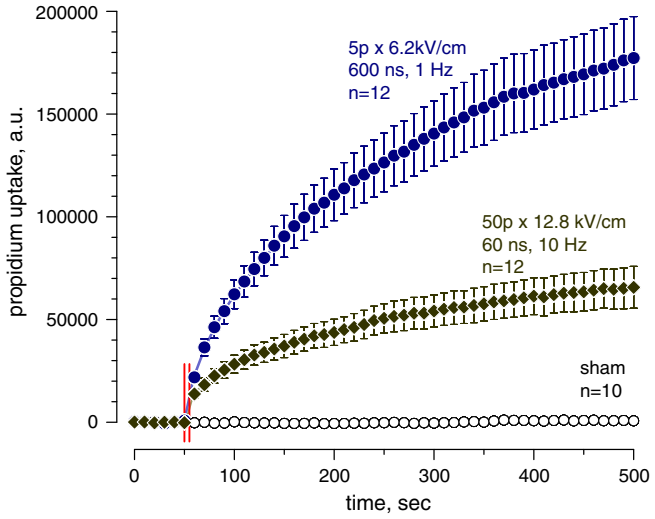

Fig. 6. Propidium uptake by cells exposed to 60- and 600-ns EP. The exposure parameters and the number of independent experiments per group are indicated next to the plots. Other details same as in Figs. 3–5.

Importantly, these larger pores were sufficiently long-lived to allow their detection by the cell volume change method. This observation supports the item (**b**) above as a more accurate interpretation of the experimental findings.

3.6. Effect of the pulsing buffer on membrane permeabilization

Multiple studies reported the enhancement of electroporation in low-conductance media, e.g., when most of NaCl is substituted with sucrose [16,51–53]. The reference buffer had about 3-fold higher conductance than all sugar- and PEG-containing buffers, so different exposure efficiency related to the pulsing buffer conductance could potentially be a confounding factor in comparing the effects in the reference buffer with the other buffers. At the same time, we did not observe medium conductance-related effects in earlier experiments with ns-duration EP which employed widely varied media [17,18,28,29]; however, these studies focused primarily on other topics. To reinforce this circumstantial evidence, now we specifically explored if a different conductance of the buffers could have contributed to studied nsEP effects.

For these experiments (Fig. 8), we used the reference buffer ("NaCl") and an isoosmotic buffer with 180 mM of sucrose ("sucrose" buffer). Cells were treated with nsEP in one of these two buffers, followed by post-exposure holding in the same buffer or in the other buffer. More details of this protocol are given in the Fig. 8 caption.

Regardless of which buffer was used for the exposure, nsEP-exposed cells displayed shrinking in the sucrose holding buffer, and swelling in the NaCl holding buffer; the magnitude and rate of the volume changes were similar. Thus, for our conditions, the extent of nsEP-induced permeabilization did not depend on which buffer was used for exposure.

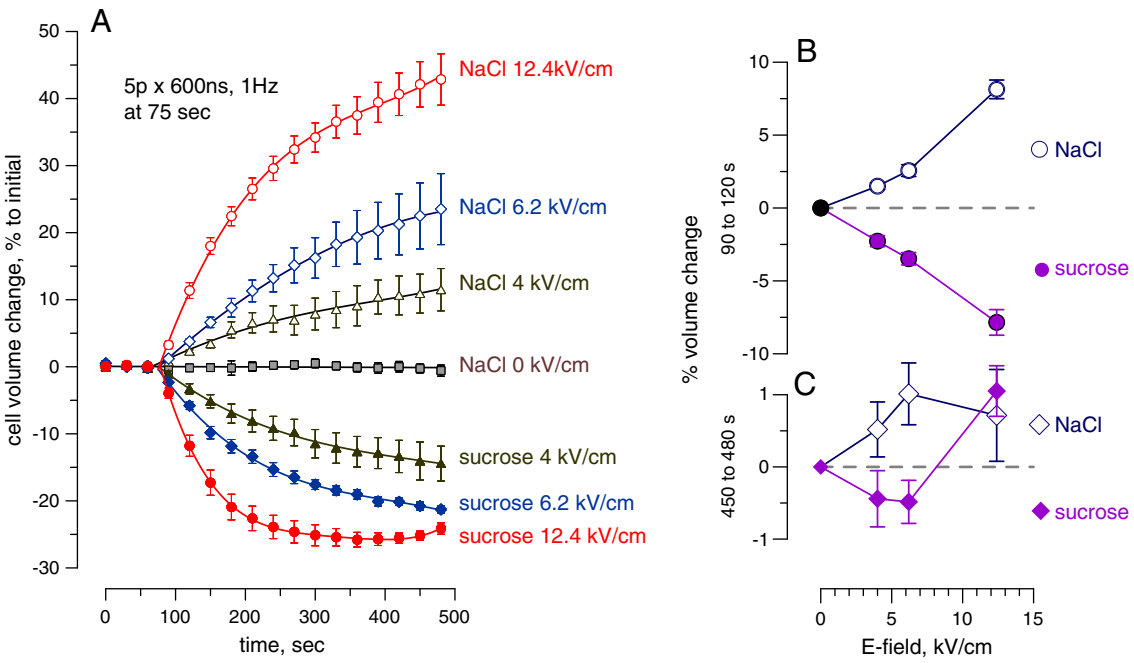

Fig. 7. Effect of the E-field intensity on cell volume changes in the reference buffer (open symbols; designated as "NaCl") and in an isoosmotic buffer with 190 mOsm/kg of sucrose instead of NaCl (solid symbols; designated as "sucrose"). Panel A shows the time dynamics of volume changes; nsEP exposure parameters are indicated on the plot. Panels B and C, respectively, show the early (90–120 s) and the late (450–480 s) rates of volume change as a function of the E-field intensity (as measured from the graphs in A). Mean ± SE, $n = 4–6$. Note the transition from shrinking to swelling in the sucrose buffer at the highest E-field intensity only ($p < 0.01$ compared to the lower E-field intensities, 2-tailed Student's t-test).

4. Discussion

We employed two different tests, namely (1) cell volume change by the colloid osmotic mechanism and (2) propidium dye uptake, to compare the populations of pores formed in cell membrane by 60- and 600-ns EP. For the cell volume experiments, we "calibrated" pore sizes by PEGs and sugars of different molecular dimensions.

The method of 3D cell volume reconstruction in individually exposed cells enabled us to reveal biphasic volume changes due to slow membrane permeation of tested solutes. The method showed

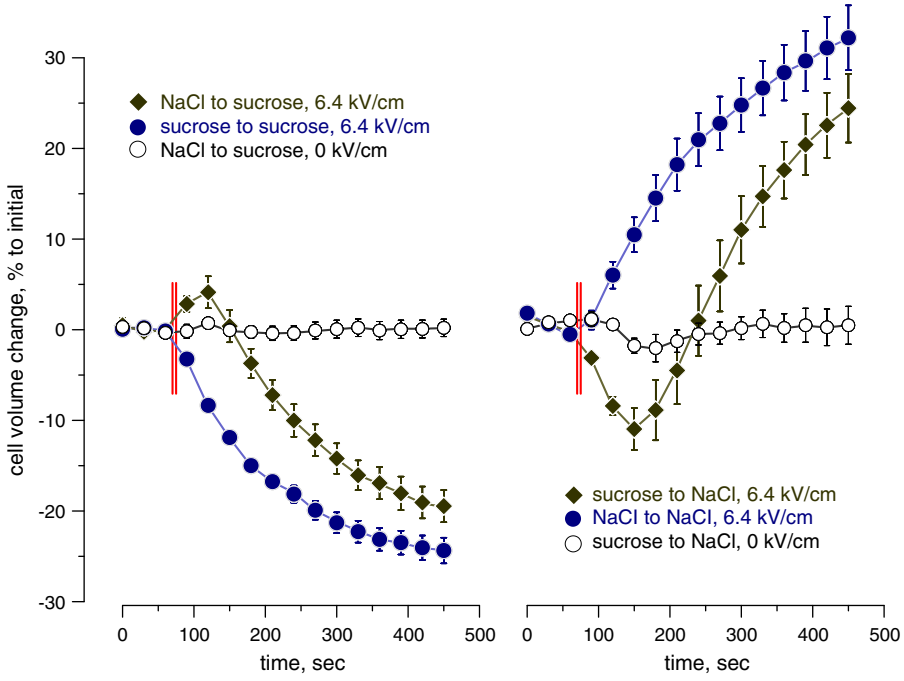

Fig. 8. Lack of the effect of the buffer composition at the time of the exposure on cell volume changes following the exposure. All experiments were performed with a continual flow of solution through the exposure bath with cells. Two different buffers were used: a reference buffer ("NaCl") and the same buffer with 100 mM of NaCl isoosmotically substituted for sucrose ("sucrose"). Cells were exposed to 5 pulses at 6.4 kV/cm, 600 ns, 1 Hz, from 70 to 75 s into the experiment (shown by vertical lines); open symbols correspond to the sham exposure data. Left panel: at 75 s, bath perfusion was switched to a the sucrose buffer (in case of sucrose to sucrose change, two different reservoirs with the same sucrose buffer were used, in order to account for possible mechanical artifacts of the flow switching). Right panel: same protocol, but at 75 s the bath perfusion was switched to the reference buffer. Mean ± SE, $n = 7–9$. Complete replacement of the buffer in the exposure bath took 30–40 s. Note that except for the delay for buffer replacement, nsEP-induced cell volume changes were determined by the buffer that was used for holding of cells after exposure.

amazingly high sensitivity, e.g., it readily distinguished between the effects of adonitol and mannitol, although these molecules have same cross-section and differ just by one carbon alcohol group (Figs. 1 and 5).

Notwithstanding its high sensitivity, the volume change method established no difference in pore populations opened by 60- and 600-ns pulses. This finding was in apparent contradiction with higher Pr uptake triggered by longer pulses (Fig. 6), which made us to hypothesize that 600-ns pulses do open larger pores, but they shrink rapidly, and therefore have little impact on the cell volume by the time of volume measurements. However, this hypothesis was challenged by finding that 600-ns pulses at 12.4 kV/cm opened larger pores than at 6.2 or 4 kV/cm, and these larger pores existed long enough to reveal sucrose uptake by biphasic volume changes (Fig. 7).

The only other way to reconcile the cell volume changes with dye uptake findings was to conclude that the fraction of Pr-permeable pores following 600-ns exposure is small when compared to the entire pore population: Whereas this pore fraction lets Pr into the cells, it has little impact on water uptake which involves all pores. In other words, the population of Pr-permeable pores was larger after the 600-ns exposure, but being just a small fraction of the entire pore population, it had little impact on the overall water uptake and volume changes. Overall, our data show that the effects of 60- and 600-ns pulses at the cellular level were qualitatively similar and even indistinguishable when using such endpoints as cell volume change.

One question that has been extensively discussed in studies with nsEP but still remains open is "what is the actual size of the nsEP-opened pores?" We do not have a straightforward answer to this question, as there is no fixed size of such pores. Instead, we can talk about a pore population with a certain pore size distribution, which depends both on the EP duration and amplitude. The data presented in Figs. 4 and 5 can be used to estimate the "effective" upper limit for pore size for the exposure conditions tested (by saying "effective," we admit that a small fraction of pores may exceed this limit, but they would play little role in cell volume changes). In Fig. 5, the ability of adonitol, mannitol, and methyl-α-D-glucoside to enter the cells is evidenced by biphasic change in the cell volume. There was no such biphasic response in sucrose and PEG 1000 buffers, indicating that these two molecules did not enter cells in any appreciable amounts. Likewise, PEG 200 and PEG 300 undoubtedly entered the nsEP-permeabilized cells, whereas PEG 400, 600, and 1000 apparently did not (Fig. 4). Hence the maximum "effective" diameter of nsEP-opened pores can be estimated as <0.9 nm from the size of the sucrose molecule (Fig. 1) or as <1.24 nm from the hydrodynamic diameter of PEG 400. Since one can speculate that PEG molecules can assume an ellipsoid shape to get into pores of a smaller radius, the pore size estimate based on the rigid structure of sugar molecules appears more accurate.

In general, findings reported in this paper using GH3 cells were consistent with our observations of cell volume changes in CHO-K1 cells [17], NG108 neuroblastoma, and U-937 monocytes (unpublished data). These studies were limited in scale and did not specifically compare the effects of 60- and 600-ns pulses, but they demonstrated nsEP-induced cell swelling and its inhibition by sucrose and PEG 1000, and also by gluconate and ascorbate anions. We infer, just as a first approximation, that within the studied limits nsEP effects on membrane pore formation in different cell lines were qualitatively similar.

As a final note, in this study we disregarded specific chemical properties of PEGs and sugars, as well as possible active volume regulation by nsEP-exposed cells. Both groups of chemicals were treated simply as osmolates, and the cell response was assumed as passive. Same as in earlier studies [7,19–21,35], we found that effects of PEGs and sugars on cell volume are consistent with what is expected based on the osmotic mechanism, whereas their specific chemical properties appear to have little effect. Likewise, we do not exclude active volume regulation by studied cells, but did not observe any effects that would need to be explained by it. In addition, earlier studies noted suppression of such regulation in electroporated cells [54], making their response more predictable from the physico-chemical point of view.

Acknowledgements

The study was supported by R01CA125482 from the National Cancer Institute, R01GM088303 from the National Institute of General Medical Sciences, and LRIR 09RH09COR from the Air Force Office of Scientific Research.

References

[1] A.G. Pakhomov, D. Miklavcic, M.S. Markov (Eds.), Advanced electroporation techniques in biology in medicine, CRC Press, Boca Raton, 2010.
[2] B. Rubinsky (Ed.), Irreversible electroporation, in: Series in biomedical engineering, Springer-Verlag, Berlin Heidelberg, 2010.
[3] E. Neumann, A.E. Sowers, C.A. Jordan (Eds.), Electroporation and electrofusion in cell biology, Plenum, New York, 1989.
[4] J. Teissie, Biophysical effects of electric fields on membrane water interfaces: a mini review, Eur. Biophys. J. 36 (2007) 967–972.
[5] J. Teissie, M. Golzio, M.P. Rols, Mechanisms of cell membrane electropermeabilization: a minireview of our present (lack of ?) knowledge, Biochim. Biophys. Acta 1724 (2005) 270–280.
[6] J.C. Weaver, Electroporation of biological membranes from multicellular to nano scales, IEEE Trans. Dielectr. Electr. Insul. 10 (2003) 754–768.
[7] U. Zimmermann, G.A. Neil (Eds.), Electromanipulation of cells, CRC Press, Boca Raton, 1996.
[8] L.M. Mir, L.F. Glass, G. Sersa, J. Teissie, C. Domenge, D. Miklavcic, M.J. Jaroszeski, S. Orlowski, D.S. Reintgen, Z. Rudolf, M. Belehradek, R. Gilbert, M.P. Rols, J. Belehradek Jr., J.M. Bachaud, R. DeConti, B. Stabuc, M. Cemazar, P. Coninx, R. Heller, Effective treatment of cutaneous and subcutaneous malignant tumours by electrochemotherapy, Br. J. Cancer 77 (1998) 2336–2342.
[9] G. Sersa, D. Miklavcic, M. Cemazar, Z. Rudolf, G. Pucihar, M. Snoj, Electrochemotherapy in treatment of tumours, Eur. J. Surg. Oncol. 34 (2008) 232–240.
[10] L.C. Heller, R. Heller, Electroporation gene therapy preclinical and clinical trials for melanoma, Curr. Gene Ther. 10 (2010) 312–317.
[11] R. Nuccitelli, X. Chen, A.G. Pakhomov, W.H. Baldwin, S. Sheikh, J.L. Pomicter, W. Ren, C. Osgood, R.J. Swanson, J.F. Kolb, S.J. Beebe, K.H. Schoenbach, A new pulsed electric field therapy for melanoma disrupts the tumor's blood supply and causes complete remission without recurrence, Int. J. Cancer 125 (2009) 438–445.
[12] L.M. Mir, Nucleic acids electrotransfer-based gene therapy (electrogenetherapy): past, current, and future, Mol. Biotechnol. 43 (2009) 167–176.
[13] G. Pucihar, T. Kotnik, D. Miklavcic, J. Teissie, Kinetics of transmembrane transport of small molecules into electropermeabilized cells, Biophys. J. 95 (2008) 2837–2848.
[14] K.J. Muller, V.L. Sukhorukov, U. Zimmermann, Reversible electropermeabilization of mammalian cells by high-intensity, ultra-short pulses of submicrosecond duration, J. Membr. Biol. 184 (2001) 161–170.
[15] J. Deng, K.H. Schoenbach, E.S. Buescher, P.S. Hair, P.M. Fox, S.J. Beebe, The effects of intense submicrosecond electrical pulses on cells, Biophys. J. 84 (2003) 2709–2714.
[16] C.S. Djuzenova, U. Zimmermann, H. Frank, V.L. Sukhorukov, E. Richter, G. Fuhr, Effect of medium conductivity and composition on the uptake of propidium iodide into electropermeabilized myeloma cells, Biochim. Biophys. Acta 1284 (1996) 143–152.
[17] A.G. Pakhomov, O.N. Pakhomova, Nanopores: a distinct transmembrane passageway in electroporated cells, in: A.G. Pakhomov, D. Miklavcic, M.S. Markov (Eds.), Advanced Electroporation Techniques in Biology in Medicine, CRC Press, Boca Raton, 2010, pp. 178–194.
[18] A.M. Bowman, O.M. Nesin, O.N. Pakhomova, A.G. Pakhomov, Analysis of plasma membrane integrity by fluorescent detection of Tl^+ uptake, J. Membr. Biol. 236 (2010) 15–26.
[19] G. Saulis, Kinetics of pore disappearance in a cell after electroporation, Biomed. Sci. Instrum. 35 (1999) 409–414.
[20] K. Kinosita Jr., T.T. Tsong, Hemolysis of human erythrocytes by transient electric field, Proc. Natl Acad. Sci. USA 74 (1977) 1923–1927.
[21] K. Kinosita Jr., T.Y. Tsong, Formation and resealing of pores of controlled sizes in human erythrocyte membrane, Nature 268 (1977) 438–441.
[22] E.H. Serpersu, K. Kinosita Jr., T.Y. Tsong, Reversible and irreversible modification of erythrocyte membrane permeability by electric field, Biochim. Biophys. Acta 812 (1985) 779–785.
[23] K.H. Schoenbach, S.J. Beebe, E.S. Buescher, Intracellular effect of ultrashort electrical pulses, Bioelectromagnetics 22 (2001) 440–448.
[24] K.S. Schoenbach, B. Hargrave, R.P. Joshi, J. Kolb, C. Osgood, R. Nuccitelli, A.G. Pakhomov, J. Swanson, M. Stacey, J.A. White, S. Xiao, J. Zhang, S.J. Beebe, P.F. Blackmore, E.S. Buescher, Bioelectric effects of nanosecond pulses, IEEE Trans. Dielectr. Electr. Insul. 14 (2007) 1088–1109.
[25] S.J. Beebe, P.M. Fox, L.J. Rec, E.L. Willis, K.H. Schoenbach, Nanosecond, high-intensity pulsed electric fields induce apoptosis in human cells, FASEB J. 17 (2003) 1493–1495.

[26] S.J. Beebe, J. White, P.F. Blackmore, Y. Deng, K. Somers, K.H. Schoenbach, Diverse effects of nanosecond pulsed electric fields on cells and tissues, DNA Cell Biol. 22 (2003) 785–796.
[27] A.G. Pakhomov, A.M. Bowman, B.L. Ibey, F.M. Andre, O.N. Pakhomova, K.H. Schoenbach, Lipid nanopores can form a stable, ion channel-like conduction pathway in cell membrane, Biochem. Biophys. Res. Commun. 385 (2009) 181–186.
[28] A.G. Pakhomov, R. Shevin, J.A. White, J.F. Kolb, O.N. Pakhomova, R.P. Joshi, K.H. Schoenbach, Membrane permeabilization and cell damage by ultrashort electric field shocks, Arch. Biochem. Biophys. 465 (2007) 109–118.
[29] A.G. Pakhomov, J.F. Kolb, J.A. White, R.P. Joshi, S. Xiao, K.H. Schoenbach, Long-lasting plasma membrane permeabilization in mammalian cells by nanosecond pulsed electric field (nsPEF), Bioelectromagnetics 28 (2007) 655–663.
[30] B.L. Ibey, S. Xiao, K.H. Schoenbach, M.R. Murphy, A.G. Pakhomov, Plasma membrane permeabilization by 60- and 600-ns electric pulses is determined by the absorbed dose, Bioelectromagnetics 30 (2009) 92–99.
[31] P.T. Vernier, Y. Sun, M.A. Gundersen, Nanoelectropulse-driven membrane perturbation and small molecule permeabilization, BMC Cell Biol. 7 (2006) 37.
[32] T.R. Gowrishankar, J.C. Weaver, Electrical behavior and pore accumulation in a multicellular model for conventional and supra-electroporation, Biochem. Biophys. Res. Commun. 349 (2006) 643–653.
[33] B.L. Ibey, A.G. Pakhomov, B.W. Gregory, V.A. Khorokhorina, C.C. Roth, M.A. Rassokhin, J.A. Bernhard, G.J. Wilmink, O.N. Pakhomova, Selective cytotoxicity of intense nanosecond-duration electric pulses in mammalian cells, Biochim. Biophys. Acta 1800 (2010) 1210–1219.
[34] R.Z. Sabirov, Y. Okada, Wide nanoscopic pore of maxi-anion channel suits its function as an ATP-conductive pathway, Biophys. J. 87 (2004) 1672–1685.
[35] V.L. Sukhorukov, D. Imes, M.W. Woellhaf, J. Andronic, M. Kiesel, R. Shirakashi, U. Zimmermann, H. Zimmermann, Pore size of swelling-activated channels for organic osmolytes in Jurkat lymphocytes, probed by differential polymer exclusion, Biochim. Biophys. Acta 1788 (2009) 1841–1850.
[36] G. Saulis, M.S. Venslauskas, J. Naktinis, Kinetics of pore resealing in cell membranes after electroporation, Bioelectrochem. Bioenerg. 26 (1991) 1–13.
[37] Y. Okada, Ion channels and transporters involved in cell volume regulation and sensor mechanisms, Cell Biochem. Biophys. 41 (2004) 233–258.
[38] S.J. Kuga, Pore size distribution analysis of gel substances by size exclusion chromatography, J. Chromatogr. 206 (1981) 449–461.
[39] R.J. Errington, N.S. White, Measuring dynamic cell volume in situ by confocal microscopy, Meth. Mol. Biol. 122 (1999) 315–340.
[40] V. Idone, C. Tam, N.W. Andrews, Two-way traffic on the road to plasma membrane repair, Trends Cell Biol. 18 (2008) 552–559.
[41] V. Idone, C. Tam, J.W. Goss, D. Toomre, M. Pypaert, N.W. Andrews, Repair of injured plasma membrane by rapid Ca^{2+}-dependent endocytosis, J. Cell Biol. 180 (2008) 905–914.
[42] B. Hille, Ionic Channels of Excitable Membranes, 3 ed.Sinauer Associates, Sunderland, MA, 2001.
[43] K. Kiyosawa, Theoretical and experimental studies on freezing point depression and vapor pressure deficit as methods to measure osmotic pressure of aqueous polyethylene glycol and bovine serum albumin solutions, Biophys. Chem. 104 (2003) 171–188.
[44] E.M. Nestorovich, V.A. Karginov, S.M. Bezrukov, Polymer partitioning and ion selectivity suggest asymmetrical shape for the membrane pore formed by epsilon toxin, Biophys. J. 99 (2010) 782–789.
[45] S.M. Bezrukov, I. Vodyanoy, V.A. Parsegian, Counting polymers moving through a single ion channel, Nature 370 (1994) 279–281.
[46] J. Sadowski, J. Gasteiger, G. Klebe, Comparison of automatic 3-dimensional model builders using 639 X-ray structures, J. Chem. Inf. Comput. Sci. 34 (1994) 1000–1008.
[47] G.J. Kleywegt, T.A. Jones, Model building and refinement practice, Meth. Enzymol. 277 (1997) 208–230.
[48] T.E. Creighton, Proteins: structures and molecular properties, 2nd ed.W.H. Freeman and Company, New York, 1993.
[49] P. Linsdell, J.A. Tabcharani, J.M. Rommens, Y.X. Hou, X.B. Chang, L.C. Tsui, J.R. Riordan, J.W. Hanrahan, Permeability of wild-type and mutant cystic fibrosis transmembrane conductance regulator chloride channels to polyatomic anions, J. Gen. Physiol. 110 (1997) 355–364.
[50] B.N. Cohen, C. Labarca, N. Davidson, H.A. Lester, Mutations in M2 alter the selectivity of the mouse nicotinic acetylcholine receptor for organic and alkali metal cations, J. Gen. Physiol. 100 (1992) 373–400.
[51] A. Ivorra, J. Villemejane, L.M. Mir, Electrical modeling of the influence of medium conductivity on electroporation, Phys. Chem. Chem. Phys. 12 (2010) 10055–10064.
[52] K. Kinosita Jr., T.Y. Tsong, Voltage-induced pore formation and hemolysis of human erythrocytes, Biochim. Biophys. Acta 471 (1977) 227–242.
[53] G. Pucihar, T. Kotnik, M. Kanduser, D. Miklavcic, The influence of medium conductivity on electropermeabilization and survival of cells in vitro, Bioelectrochemistry 54 (2001) 107–115.
[54] M. Usaj, K. Trontelj, R. Hudej, M. Kanduser, D. Miklavcic, Cell size dynamics and viability of cells exposed to hypotonic treatment and electroporation for electrofusion optimization, Radiol. Oncol. 43 (2009) 108–119.